Journal of Volcanology and Geothermal Research 304 (2015) 82–93

Contents lists available at ScienceDirect

Journal of Volcanology and Geothermal Research

journal homepage: www.elsevier.com/locate/jvolgeores

Characterising volcanic cycles at Soufriere Hills Volcano, Montserrat: Time series analysis of multi-parameter satellite data

Verity J.B. Flower *, Simon A. Carn

Dept. of Geological and Mining Engineering and Sciences, Michigan Technological University, 1400 Townsend, Dr, Houghton, MI 49931, USA

ARTICLE INFO

Article history:
Received 6 April 2015
Accepted 30 July 2015
Available online 11 August 2015

Keywords:
A-Train
OMI
MODIS
Volcanic cycles
Soufriere Hills Volcano

ABSTRACT

The identification of cyclic volcanic activity can elucidate underlying eruption dynamics and aid volcanic hazard mitigation. Whilst satellite datasets are often analysed individually, here we exploit the multi-platform NASA A-Train satellite constellation to cross-correlate cyclical signals identified using complementary measurement techniques at Soufriere Hills Volcano (SHV), Montserrat. In this paper we present a Multi-taper (MTM) Fast Fourier Transform (FFT) analysis of coincident SO_2 and thermal infrared (TIR) satellite measurements at SHV facilitating the identification of cyclical volcanic behaviour. These measurements were collected by the Ozone Monitoring Instrument (OMI) and Moderate Resolution Imaging Spectroradiometer (MODIS) (respectively) in the A-Train. We identify a correlating cycle in both the OMI and MODIS data (54–58 days), with this multi-week feature attributable to episodes of dome growth. The ~50 day cycles were also identified in ground-based SO_2 data at SHV, confirming the validity of our analysis and further corroborating the presence of this cycle at the volcano. In addition a 12 day cycle was identified in the OMI data, previously attributed to variable lava effusion rates on shorter timescales. OMI data also display a one week (7–8 days) cycle attributable to cyclical variations in viewing angle resulting from the orbital characteristics of the Aura satellite. Longer period cycles possibly relating to magma intrusion were identified in the OMI record (102-, 121-, and 159 days); in addition to a 238-day cycle identified in the MODIS data corresponding to periodic destabilisation of the lava dome. Through the analysis of reconstructions generated from cycles identified in the OMI and MODIS data, periods of unrest were identified, including the major dome collapse of 20th May 2006 and significant explosive event of 3rd January 2009. Our analysis confirms the potential for identification of cyclical volcanic activity through combined analysis of satellite data, which would be of particular value at poorly monitored volcanic systems.

1. Introduction

The identification of cyclical activity on various timescales at active volcanoes has been used to draw conclusions about the subsurface processes driving these systems (Spampinato et al., 2012; Costa et al., 2013) and can also inform volcanic hazard assessment. Factors such as cycle duration and volume of erupted material have been assessed through modelling to infer the size and structure of subsurface features such as magma chambers and conduits (Costa et al, 2007; Lensky et al., 2008). However, to identify these cycles a time-series dataset of significant duration and resolution is required, which can be difficult to obtain for remote or unmonitored volcanoes. In these situations measurements by operational satellite instruments can constitute an invaluable resource, and since the advent of daily, global measurements of volcanic sulphur dioxide (SO_2) by sensors such as the Ozone Monitoring Instrument (OMI; Carn et al., 2013) the collection of SO_2 data for persistently degassing volcanoes has become routine (e.g., Carn et al., 2013; McCormick et al., 2012). These SO_2 observations complement long-term thermal infrared (TIR) measurements that have been collected for more than a decade by sensors such as the Moderate Resolution Imaging Spectroradiometer (MODIS; e.g., Wright et al., 2002). In this contribution we test the feasibility of using time-series satellite measurements to identify cyclical activity at persistently active volcanoes.

We posit that synergistic analysis of multiple satellite datasets (e.g., SO_2 and TIR data) to assess eruption dynamics will result in a more robust interpretation of the nature of the volcanic activity, by reducing the impacts of individual sensor limitations, and providing coincident information on fluxes of SO_2 and TIR radiance. Daily, near-coincident, multi-spectral observations have been provided since 2004 by NASA's A-Train satellite constellation, consisting (in February 2015) of the GCOM-W1, Aqua, CALIPSO, Cloudsat and Aura platforms (NASA, 2010). SO_2 can be measured remotely due to significant absorption bands in the ultraviolet (UV) portion of the electromagnetic spectrum (Platt and Stutz, 2008; Yang et al., 2009). NASA's Aura satellite, launched

* Corresponding author.
E-mail address: vjflower@mtu.edu (V.J.B. Flower).

http://dx.doi.org/10.1016/j.jvolgeores.2015.07.035

in 2004, carries the UV–Visible OMI sensor currently used to measure multiple atmospheric trace gases including SO_2 (Carn and Prata, 2010; Krotkov et al., 2006, 2010; Prata et al., 2007; Yang et al., 2007). The detection of surface thermal anomalies or 'hotspots' is facilitated by MODIS, using radiance measurements in multiple bands of the short-wave IR (SWIR) and TIR (Wright et al., 2002). MODIS instruments are flown on-board NASA's Terra and Aqua satellites, and since September 2004 Aqua/MODIS has provided daytime TIR observations coincident with Aura/OMI SO_2 measurements. The presence of OMI and MODIS in the A-Train permits cross-correlation due to the fixed orbital formation of the Aura and Aqua satellites, with no more than a 15-min lag between the measurements collected by the overpass of the first (Aqua) and last (Aura) satellites.

The combination of SO_2 and TIR measurements should permit the identification of a wider variety of volcanic activity types than either dataset in isolation. For example, whilst an ongoing effusive eruption may feature minimal variation in SO_2 mass loadings and therefore a constant SO_2 emission rate, the corresponding TIR measurements may vary due to the development of lava flows from surface to tubular flow features (Koeppen et al., 2011). Additionally vigorous degassing may produce opaque plumes that could obscure subjacent thermal features (e.g., active lava lakes or domes), and thus potentially result in anti-correlations between SO_2 emissions and TIR radiance. Based on any co-variations in the two datasets we aim to identify the types of activity that may be occurring (e.g. lava dome growth, waxing/waning of lava lakes). By identifying dominant cycles we aim to provide insight into not only the processes occurring but also the timescales upon which certain forms of activity are likely to reactivate.

We use Soufriere Hills volcano (SHV; Montserrat) as an initial test of the viability of this methodology, as a similar analysis was applied to ground-based gas measurements at SHV in 2002–2009 by Nicholson et al. (2013), thus providing some independent validation. For consistency with Nicholson et al. (2013), we focus on coincident OMI and MODIS data collected between January 2005 and December 2009, which encompasses three phases of lava dome growth at SHV: August 2005–April 2007, July 2008–January 2009 and October 2009 (Wadge et al., 2010). An additional motivation for selecting this timeframe is minimisation of the impacts of data gaps caused by the OMI Row Anomaly (ORA; see Section 2.1). For comparative purposes, Table 1 lists previous studies that have identified cycles in datasets from SHV as well as the identified source of each cycle. In addition to the observed cycles identified at SHV, Carn et.al. (2007) identified the possible presence of a 6-day cycle in OMI SO_2 measurements induced by the cyclical divergence of the viewing angle from nadir. In addition to this, the orbital path of the A-Train results in variations of viewing angle for fixed targets with a repeat cycle of 16 days. Hence, in order to identify cycles relating to volcanic processes in satellite measurements, we first identify and eliminate any signal modulations due to instrumental or other non-volcanic sources.

Table 1
Cycles identified in previous studies of Soufriere Hills Volcano, Montserrat.

Reference	Data type	Cycle period(s)
Odbert et al., 2014	Review of previous work: Seismic, lava flux, observations,	Sub-daily Sub-annual Multi-annual Multi-decadal
Lamb et al., 2014	Earthquakes	~200 days ~100 days ~50 days
Costa et al., 2013	Combined model and seismic data	40 days
Vitturi et al., 2013	Deformation, seismic and visual observations	4–36 h 5–7 weeks
Michaut el al., 2013	Deformation	6–30 h
Nicholson et al., 2013	Ground-based DOAS SO_2	171 days 54 days 19 days 12 days 8 days
Loughlin et al., 2010	Discharge pulse and rockfall events	2–6 weeks 11–16 days
Wadge et al., 2010	Identified short period pulses in lava flux	10–15 days
Odbert and Wadge, 2009	Lava flux and deformation data	10 h 50 h
Elsworth et al., 2008	Observations	2–3 years (interspersed by 1.5-2 year)
Costa et al., 2007	Model of dyke embedded in elastic media	38–51 days (i.e., 5–7 weeks)
Jaquet et al., 2006	Coupled seismic and model data	40 days
Melnik and Sparks, 2005	Models	6–7 weeks
Carn et al., 2004	Observations	7–10 h
Edmonds et al., 2003	SO_2 emissions post-rockfalls and pyroclastic flows	60–180 min
Druitt et al., 2002	Deformation and seismic	2.5–63 h (av. 10 h)
Sparks and Young, 2002	Observed resurgence of lava extrusion (1997)	36–52 days
Watson et al., 2000	Deformation, seismic and gas	8–14 h
Denlinger and Hoblitt, 1999	Deformation and seismic	4–30 h
Voight et al., 1999	Deformation	6–30 h
Voight et al, 1998	Deformation	6–18 h

2. Data

2.1. OMI SO_2 measurements

Operational OMI SO_2 measurements (Yang et al., 2007) comprise the primary dataset for this analysis since they provide a ~10-year record of daily, global SO_2 observations, and sensitivity to lower tropospheric volcanic SO_2 emissions (i.e., passive degassing; Carn et al., 2013). Currently, daily OMI SO_2 data for volcanic regions can be viewed on the Global Sulfur Dioxide Monitoring website at NASA Goddard Space Flight Center (http://so2.gsfc.nasa.gov) and the Support to Aviation Control Service website (http://saca.aeronomie.be/nrt). For our quantitative analysis of SO_2 emissions we use the operational Level 2 OMI Sulphur Dioxide product (OMSO2 collection 3), which is publicly available from the NASA Goddard Earth Sciences (GES) Data and Information Services Center (DISC; http://disc.sci.gsfc.nasa.gov/Aura/data-holdings/OMI/omso2_v003.shtml). In order to analyse SO_2 emissions from SHV, OMSO2 data were extracted from a 4° × 4° latitude-longitude box (~450 × 450 km) centred over the volcano. Since SO_2 retrievals depend on the assumed altitude of the gas, the OMSO2 data product includes three volcanic SO_2 column amounts retrieved assuming different a-priori SO_2 plume altitudes (~3, ~8 and ~17 km; Carn et al., 2013). Recorded plume heights at SHV in the 2005–2009 period (Global Volcanism Program, 2009) indicate that plumes were typically confined to the lower troposphere (~1.5–4 km altitude), and hence we use the lower tropospheric (TRL) SO_2 columns which assume a SO_2 plume altitude of ~3 km (Carn et al., 2013). Overestimation of SO_2 altitude leads to underestimation of SO_2 column amounts and vice versa; based on linear interpolation of OMI TRL and mid-tropospheric (TRM; ~8 km SO_2 altitude) SO_2 columns we estimate that SHV plume altitude variations in the 1.5–4 km range would result in up to ~20% variation in SO_2 mass. Sources of error in the operational OMI SO_2 measurements (including SO_2 profile, non-linear absorption and cloud effects) are also discussed by Yang et al. (2007), who estimate an overall uncertainty of 20%. In the case of SHV we expect meteorological clouds to be the most significant source of error, assuming that there are relatively minor variations in the SO_2 profile (i.e., plume altitude) and negligible non-linear absorption effects due to low SO_2 column amounts in the SHV plume. Variability in the measured SO_2 mass can also result from the variation in OMI pixel size or GIFOV (ground-projected instantaneous field of view) during the 16-day Aura repeat cycle (Krotkov et al, 2006). The effect is most pronounced for sub-pixel sized SO_2 plumes which are averaged over the OMI GIFOV. In order to better

resolve smaller plumes an instrument with higher spatial resolution would be necessary, but a significant increase in spatial resolution (i.e., to sub-km scale) would be accompanied by a decrease in temporal resolution, limiting the accurate identification of volcanic cycles. OMI measurements offer a combination of daily global coverage and high SO_2 sensitivity that is favourable for application of time-series analysis techniques.

An additional source of error exists in OMI data obtained since 2008 due to the OMI Row Anomaly (ORA), a blockage in the sensor's field of view (FOV) that results in periodic data gaps (see: http://www.knmi.nl/omi/research/product/rowanomaly-background.php). Inspection of daily OMI SO_2 imagery (e.g., http://so2.gsfc.nasa.gov) shows that the ORA impacts locations approximately every 2–8 days, with the extent of the anomaly being somewhat unpredictable until its stabilisation in July 2011. To minimize the impact of the ORA, we restrict our analysis to time periods prior to, or early in the development of the ORA when data gaps were relatively small in extent.

2.2. MODIS thermal IR data

MODIS TIR data were compiled from the MODVOLC web-based thermal alert system (Wright et al, 2004; http://modis.higp.hawaii.edu/). MODVOLC output consists of spectral radiance recorded in 5 MODIS bands (at wavelengths of 3.96, 1.64, 11.03, and 12.02 μm) for all thermally anomalous pixels (volcanic and non-volcanic). MODIS channels 21 and 22 both cover the 3.96 μm spectral band but with different dynamic ranges and hence saturation temperatures. We use Band 22 radiances unless the saturation temperature (~330 K) was reached, in which case the radiance from Band 21 was used. The MODVOLC database incorporates anomalies from both Terra/MODIS (since 1999) and Aqua/MODIS (since 2002), providing combined coverage of four MODIS observations per day (1 daytime and 1 night-time acquisition per satellite) with increasing coverage at higher latitudes. As with the SO_2 measurements, the MODIS viewing angle impacts the GIFOV and therefore can introduce radiance variations with relative position across the swath, due to spatial averaging of sub-pixel sized radiant heat sources (e.g., Wooster et al., 1998). Additional sources of uncertainty include the obstruction of hot features (e.g., the SHV lava dome) confined within summit craters (depending upon the viewing angle) or by meteorological clouds, and pixel geolocation errors of up to ~2 km (Wright et al., 2004). To account for this uncertainty, MODVOLC alerts located up to 2 km from the terminus of known activity (e.g. pyroclastic flows, lahars) at SHV were included in the analysis; thus encompassing alerts associated with rockfalls or pyroclastic flows from the SHV dome. Additional noise in daytime MODIS data results from reflected sunlight (increased diffuse background radiation over land), surface heating (increases in emitted background radiance) and sun glint (intense specular reflection from bodies of water), necessitating a higher alert threshold in the MODVOLC daytime algorithm (Giglio et al., 2003; Wright et al., 2002, 2004) which can lead to differences in the number and intensity of anomalies registered under these varying conditions (e.g., Fig. 1). The variable alert threshold reduces false alerts but also results in suppression of lower intensity hotspots (Wright et al., 2002, 2004), especially in daytime data, and hence could represent a significant source of error in this analysis.

3. Time-series analysis methodology

3.1. Data compilation

Daily OMI SO_2 mass and MODIS Band 22/21 radiance data were compiled for SHV where available in 2005–2009 (Fig. 1). In the OMI time-series, data gaps exist due to periodic switching of the instrument to spatial zoom mode (once per month), or temporary instrument outages (periods of no OMI data availability); these are identified in Fig. 1A. In addition, the presence of meteorological clouds impacts volcanic plume detection depending on the relative altitude of the SO_2 and the meteorological clouds. If optically-thick cloud is present above the SO_2 plume it will likely prevent detection of SO_2 in addition to any thermal anomaly; clouds beneath the plume would enhance the SO_2 signal but still mask any TIR radiance. The significance of these data gaps was assessed to establish the level of required pre-analysis correction (e.g., data gap padding). Data gap padding facilitates the use of time series analysis techniques requiring continuous, uniformly sampled data. Due to the dynamic nature of volcanic systems and the variability of interference from features such as meteorological clouds, missing data were replaced by zero values. This process was applied in favour of padding with a mean value, as it facilitated the identification of cycles induced by interference factors, including those related to seasonal variability in meteorological cloud cover obscuring the SHV SO_2 plume or lava dome. In contrast the automated nature of the MODVOLC system limits MODIS data availability to periods when the algorithm identifies a thermal anomaly, preventing further investigation into the specific cause of a particular data gap (e.g. incomplete global coverage achieved in equatorial regions, instrument outage, cloud coverage, no identified anomalies present).

Following initial assessment of the OMI time-series, we found that the OMI analysis domain (450 km square region centred over SHV) permitted detection of passively degassed SO_2 plumes confined to the immediate area around Montserrat, but missed larger emissions associated with some dome collapse or explosive events. The latter are injected higher into the atmosphere and are typically transported rapidly away from the volcano, beyond the domain used for OMI SO_2 data analysis, and are therefore omitted from the time-series, potentially influencing the cycles resolved in the MTM analysis. Four instances of large SO_2 emissions associated with dome collapses (20th May 2006) and explosive events (8th Jan 2007, 29th July 2008 and 3rd Jan 2009) were identified, and estimates of SO_2 loading from Carn and Prata (2010) were incorporated into the OMI dataset by replacing the individual value obtained for each day in the original compiled data series (Fig. 1A). We also note that these large, instantaneous SO_2 emissions were not factored into the analysis of Nicholson et al. (2013), since they are not captured by the ground-based DOAS SO_2 monitoring network at SHV.

The complete daily time-series of OMI and MODIS data were divided into specific subsets for time-series analysis; separating observations by platform and time of measurements and segregation based upon SHV's eruption history. During the operational period of Aura and Aqua four periods of heightened activity (i.e., lava dome growth) at SHV occurred: Phase 3 (1 August 2005–20 April 2007), Phase 4 (28 July 2008–3 January 2009; consisting of two, month-long phases of extrusion 3 months apart; Wadge et al., 2014) and Phase 5 (October 2009–February 2010). To facilitate the identification of longer cycles, a single continuous period was selected encompassing the majority of these phases covering 1 January 2005–31 December 2009 with the remaining available data being analysed for comparative purposes. In addition, excluding post-2009 data reduces the impact of the ORA, as this feature developed from 2008. The segregation of MODVOLC data based on measurement characteristics, which facilitated the comparison of coincident measurements from Aura/OMI and Aqua/MODIS, also allowed the selection and investigation of the remaining Aqua/MODIS night-time IR data (which has greater sensitivity to thermal anomalies).

3.2. Spectral and statistical analysis

The daily sampling rate of OMI and MODIS over the period of study (2005–2013) produced 3102 data points. These were subsequently divided into dome forming (pre-February 2010) and post-dome forming (post-February 2010) periods comprising 1826 and 1276 data points, respectively. Data gaps (Fig. 1) were padded with zero values to permit analysis as a continuous time series, with the number of

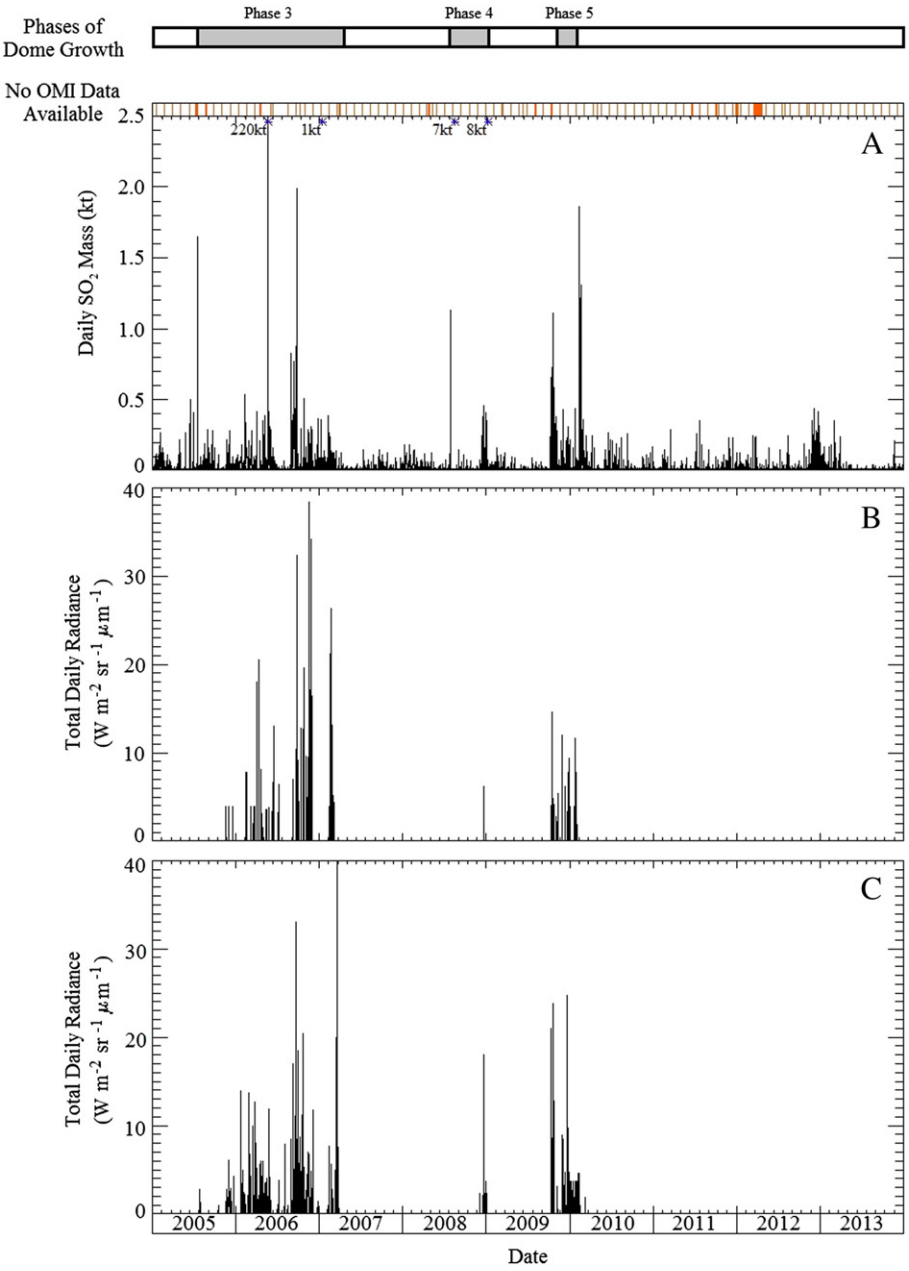

Fig. 1. Total daily SO_2 mass measured at SHV within defined analysis regions (2005–2013), with eruption phases indicated above: A) OMI SO_2 mass from the standard analysis region with additional data points (*) and corresponding SO_2 loadings from Carn and Prata (2010). OMI data gaps are indicated above the OMI time-series; B) daytime radiance from Aqua/MODIS; C) night-time radiance from Aqua/MODIS.

gaps in the total, dome forming and post-dome forming phases being 176, 81 and 95, respectively.

The compiled OMI and MODIS data were analysed utilising time-series analysis techniques to estimate Power Spectral Density (PSD; signal power as a function of frequency) and statistical methods to assess the significance of PSD maxima. For consistency with Nicholson et al. (2013), we applied the Multi-Taper Method (MTM) (Thomson, 1982) using Interactive Data Language (IDL) software available through the University Corporation for Atmospheric Research (UCAR) archive (http://download.hao.ucar.edu/oldpub/green/chromo/PROGRAMS) to estimate the PSD of the OMI and MODIS time-series. The time-series data were detrended prior to analysis, and data gaps padded with zero values to create the required length for analysis (data length must be equal to 2^n where n is an integer (Thomson, 1982)). The MTM technique has also been favoured for analysis of other geophysical signals, including atmospheric, oceanic, paleoclimate, geochemical tracer and seismological data (e.g., Mann and Lees, 1996). MTM minimises spectral leakage through the convolution of the data with a complimentary set of taper functions before PSD calculation, additionally reducing aliasing within the data. This technique is most appropriate when the dynamics of the source are undefined (Percival and Walden, 1993) and results indicate both the strength and frequency of cycles present in the data, which may otherwise be obscured by environmental and instrumental noise (e.g., seasonal variations and variable viewing geometry). To assess the significance of the identified cycles, we attempted to determine the type of noise present in the data in order to constrain appropriate confidence levels with which to identify significant peaks in the PSD output. Initial assessment compared the data to both a red noise model (Mann and Lees, 1996) and white noise limits (Duchon and Hale, 2012) in order to establish the general structure. Application of the red noise model resulted in a majority of the high frequency cycles present surpassing the imposed confidence limits, whereas only single

defined peaks exceeded the white noise model limits; hence the latter was selected for implementation. However, since both analyses resulted in the identification of cycles surpassing the respective confidence limits, we assume that the time series contains elements diverging from the background noise level of the measurements. Any PSD peaks surpassing the imposed white noise confidence limits (95% and 99%) were investigated in an attempt to identify their generating source (e.g. volcanic, meteorological, or instrumental).

Following PSD analysis, the dominant cycles were isolated using band-pass filters, which facilitate the selection of a defined frequency range whilst disregarding signals above or below the imposed limit (Duchon and Hale, 2012). Through the use of an inverse FFT analysis, the selected MTM FFT signal was then converted back into the time domain allowing plotting of isolated cycles over the time period of the original satellite observations. This method of selecting and displaying cycles in the original data results in the preservation of the relative magnitude and offset characteristics of the cycle, however as the selected signal directly relates to the time series analysed it can only be displayed over the time period of the input data. This method requires visual assessment of the resulting signal to ensure that an appropriate selection was made, as if the frequency range selected is too small, no signal will be resolved, whilst definition of a large band of frequencies will result in the selection of multiple signals which will not display the sinusoidal characteristics of a single cycle component.. When dealing with the reconstruction of signals generated by volcanic processes, assessment of the relative magnitudes of component cycles is imperative; our method facilitates incorporation of the individual characteristics (e.g., amplitude, temporal offset) of selected cycles. Once selected, the individually identified cycles were combined into a single reconstruction of the dominant cycles present at SHV. Following normalisation, the combined signal was then superimposed onto the original SO_2 or TIR time-series data, facilitating comparison of the reconstruction with the original time series observations. This approach differs from previous work by Nicholson et al. (2013), which involved the artificial creation of identified cycles and relied on statistical tests such as least-squares regression to assess the relative significance of each cycle. Once these individual cycles were modelled, Nicholson et al. (2013) performed visual assessment of best fit to validate the position of peaks of the resulting cycles against the original data.

4. Results

The results of the coincident OMI (Section 4.1) and daytime MODIS (Section 4.21) analysis for SHV are discussed in the following sections along with a comparative analysis of the filtered daytime MODIS data and the remaining night-time MODIS time-series (Section 4.22).

4.1. OMI

MTM analysis of OMI SO_2 data was conducted on the full SHV time-series (January 2005-June 2013; Fig. 2A) and on multiple smaller time windows (Fig. 2; Table 2). Activity at SHV varied significantly during the 2005–2013 period (Fig. 1), with multiple phases of active lava dome growth interspersed with periods of quiescence (e.g., Wadge et al., 2010), although SO_2 emissions have been continuous throughout (Christopher et al, 2010). The data were split accordingly into a period of intermittent active dome growth (2005–2009) and a post-dome growth period (2010–2013) and the analysis repeated (Fig. 2B, C; Table 2). This reduces the confidence in lower frequency cycles due to a reduction in the number of cycles that can occur within the selected time window, therefore a limit of detection (LOD) was established as a cycle period of $n/4$ days, where n is the total number of samples analysed (Duchon and Hale, 2012).

Prior to 2010 a greater number of cycles surpassing the confidence limits were identified (Fig. 2B), relative to the period after dome growth had ceased (Fig. 2C). The magnitude of activity after 2010 (SO_2 emissions and TIR anomalies) is visibly reduced (Fig. 1) compared to the dome-forming phase (2005–2009), and this reduction in activity corresponds to a decrease in signal strength in the MTM analysis. If cyclic behaviour at SHV is primarily associated with dome forming activity, then we would expect a decrease in the number and strength of cycles concomitant with a reduction in activity at SHV, as is the case here. Analysis of day and night-time MODIS data for the dome-forming phase was also completed, allowing identification of dominant cycles (Table 2) for selection and reconstruction of the signal and investigation of their potential causes (Table 3).

4.2. MODIS

4.21. Daytime analysis

As with the OMI analysis, a white noise model was found to be most appropriate for the definition of confidence limits for cycle identification in MODIS data at SHV (Fig. 3). Most of the signal components identified in the analysis of the complete MODIS time-series (2005–2013) were contributed by signals present prior to 2009, with minimal significant signals identified in the post-2009 assessment (Table 2). This is most likely due to the cessation of dome growth in early 2010, resulting in no thermal anomalies detected after March 2010 (Fig. 1) preventing cycle assessment. The MODIS analysis indicates a dominance of higher frequency cycles (period of ~2.3 days) than those identified in the OMI SO_2 analysis (Table 2), however the two datasets show broadly similar cyclicity with cycles present at periods of ~165 and ~55 days.

4.22. Night time comparison

The night-time MODIS data analysis favoured the identification of lower frequency cycles over the daytime analysis (Fig. 3), with three significant cycles within the LOD and displaying greater than 99% significance (periods of 238, 172, and 58 days; Fig. 3b, Table 2). MTM analysis was also completed on a combined time-series containing all Aqua/MODIS thermal anomalies, with the results dominated by the low frequency cycles identified in the night-time analysis. We attribute this to the increased sensitivity of the night-time MODVOLC algorithm (Section 2.2), producing a stronger signal than the corresponding daytime measurements.

4.3. Time-series reconstruction

4.31. OMI

The PSD analysis of OMI data for the active dome-forming phase at SHV (2005–2009) identified one peak below the LOD and surpassing the 99% confidence limit (corresponding to a cycle with a period of 159 days; Fig. 2B, Table 2). Additionally, 14 cycles were identified surpassing the 95% confidence limit, ten of which are shorter than the repeat cycle of the satellite platform (16 days) and therefore must be interpreted with caution. The remaining cycles were investigated and possible causes are suggested in Table 3. Four cycles were considered for inclusion in a time-series reconstruction (periods of 121, 55, 159 and 102 days; in order of significance) in addition to investigation of the 12.8 day cycle, which is similar to that identified by Nicholson et al (2013). These cycles were isolated using a band-pass filter (Section 3.2) and incorporated into the reconstruction analysis (Fig. 4).

The combined signal was normalised and overlaid on the original OMI SO_2 time-series (Fig. 4). Increases in the observed SO_2 emissions early in the analysis period (February 2005, June–July 2005, November 2005-February 2006, May 2006 and September 2006-January 2007) correspond to coeval increases in the reconstructed signal, particularly in the first half of the time-series in January 2005-March 2007 (Fig. 4). Later in the analysis period, some peaks in the reconstruction do not correspond to observed increases in SO_2 loading, or the magnitude of the observed increase in SO_2 mass is smaller relative to the reconstructed peak; e.g., April–June 2007 and April–August 2009. The

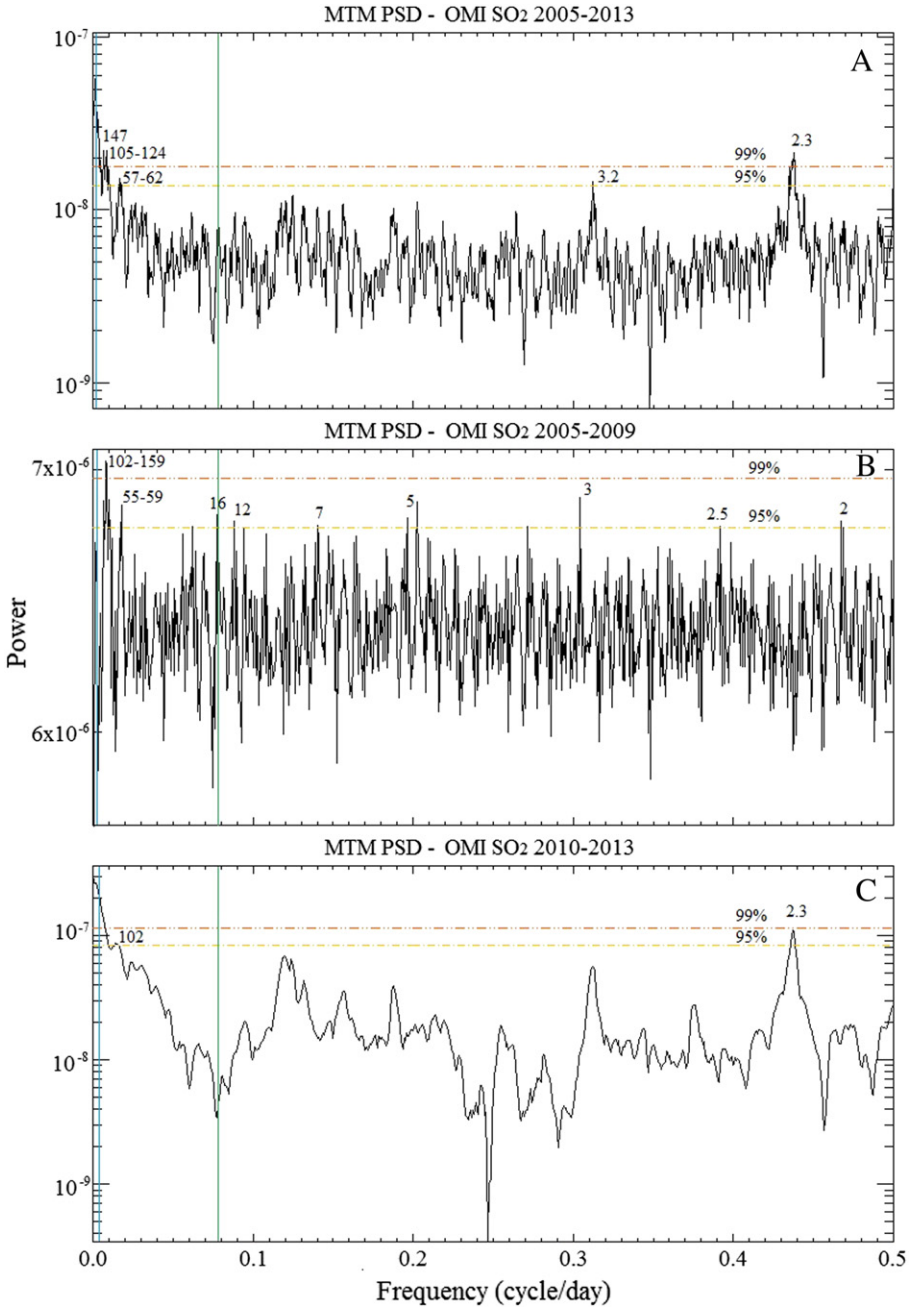

Fig. 2. MTM PSD plots of OMI SO_2 data with 95% and 99% confidence levels for: A. Entire time-series (January 2005–December 2013); B. Intermittent dome-forming eruption phase including additionally identified points (2005–2009); C. Post-dome forming phase (2010–2013). LODs (-) of 800, 450 and 320 days, respectively, are included in (A), (B) and (C) to indicate the maximum length of cycle considered. The satellite repeat cycle (16 days) is also indicated (-), as shorter-period (higher frequency) cycles could be artefacts of the measurement technique and hence require greater scrutiny.

identified cycles seem to reproduce the general dynamics of SO_2 emissions prior to the major SHV dome collapse in May 2006, in addition to resolving the decrease in SO_2 emissions following this event (Fig. 4). The increase in the reconstructed signal in May 2006 is the result of constructive interference of all 4 component cycles (55, 102, 121 and 159 days) with the decrease following the May 20, 2006 dome collapse correlating with a minimum in the 121-day cycle followed ~10 days later by combined minima in both the 55- and 159-day cycles. Also replicated is the one-month reduction in signal in December 2007 resulting from coincident minima in the 102- and 159-day cycles.

The direct influence of the 159-day cycle prompted investigation into meteorological cloud coverage as a possible cause of this cycle, as we suggest for the 172–182 day cycles identified in the MODIS data (Section 4.32). Using the OMI cloud fraction parameter, we assessed the location and extent of meteorological cloud cover on individual days during periods of minimal forcing of this cycle (i.e., when a higher number of cloud-affected days would be expected). These periods appear relatively stable, with only one displaying more than 5 days of significant cloud coverage; and we therefore tentatively conclude that the signal is more likely of volcanic rather than meteorological origin.

Elevated SO_2 loadings were identified from September–October 2008 with a reduction in the signal in November 2008 (Fig. 4). Through analysis of the individual component cycles, we posit that the reduction in signal is the result of coincident minima in both the 55- and 121-day cycles. Since these cycles are both attributable to volcanic processes (Table 3), this reduction in emissions appears to be of volcanic origin. The short dome-forming phase in late 2008 (December 2008–January 2009) is accompanied by an increase in SO_2 loadings, and it is resolved

Table 2
Cycles identified in MTM analysis of OMI and MODIS data.

Date range (data points)	OMI analysis			Daytime MODIS			Night-time MODIS		
	Peak frequency (cycle/day)	Peak period (days)	Sig (%)	Peak frequency (cycle/day)	Peak period (days)	Sig (%)	Peak frequency (cycle/day)	Peak period (days)	Sig (%)
1st January 2005–	0.0012	833[a]	99	0.0006	1667[a]	99	–	–	–
31st December 2013	0.0068	147	99	0.0030	333	95			
(3102)	0.0081	124	99	0.0089	112	95			
	0.0095	105	99	0.0121	83	95			
	0.0160	62	95	0.1840	5.43	95			
	0.0175	57	95	0.2202	4.54	95			
	0.3119	3.2	95	0.4197	2.38	95			
	0.4350 0.4378	2.3 2.28	99	0.4250	2.35	99			
			99	0.4378	2.28	99			
1st January 2005–	0.0062	159	99	<0.002	>500[a]	99	<0.001	>1000[a]	99
31st December 2009	0.0086	121	95	0.0055	182	95	0.0042	238	99
(1826)	0.0098	102	95	0.0135	74	95	0.0058	172	99
	0.017	58.8	95	0.0184	54	95	0.0142	70	95
	0.0179	55.8	95	0.1665	6.01	95	0.0153	65	95
	0.0617	16.21	95	0.4198	2.38	95	0.0170	58	99
	0.0779	12.88	95	0.4256	2.34	99			
	0.088	11.36	95	0.4380	2.28	99			
	0.1401	7.14	95						
	0.1968	5.08	95						
	0.2024	4.94	95						
	0.2718	3.68	95						
	0.304	3.29	95						
	0.3919	2.55	95						
	0.4675	2.14	95						
1st January 2010–	0.0098	102	95	0.0098	102	95	–	–	–
31st December 2013	0.4370	2.29	95	0.4370	2.29	95			
(1276)									

[a] Cycles outside LOD.

by the reconstruction analysis (Fig. 4); eruption reports indicate that this period was initiated by an explosion accompanied by a small dome collapse and the development of pyroclastic density currents (Wadge et al., 2014). This triggered an increase in the lava extrusion rate and subsequent activity was characterised by a series of explosions culminating in early January 2009 with a series of major explosions followed by a significant decrease in activity (Komorowski et al., 2010). There followed an extended period of quiescence (February–October 2009) during which time the system may have been readjusting, which could explain the observed discordance with the reconstruction of dominant cycles in this analysis (Fig. 4), before the onset of another period of dome growth in October 2009. More accurate reconstruction of the SO_2 data would require the inclusion of the shorter-period cycles disregarded in this analysis, in addition to activity with a characteristic timescale greater than the LOD constrained by the temporal extent of currently available satellite data. However, we find that through the selection of a few dominant cycles the general dynamics of the SHV system can be adequately reconstructed.

MTM analysis of ground-based SO_2 measurements at SHV in 2002–2011 by Nicholson et al. (2013) indicated, using least-squared regression, that a 54-day cycle was present, although their reconstruction was subsequently weighted in favour of other identified cycles with periods of 8- and 11 days. Our analysis reveals corresponding cycles (to within ~1 day) in the OMI SO_2 data (Table 2; Fig. 2), with the 54-day cycle (attributed to extrusion of a dyke embedded in an elastic medium; Sparks and Young, 2002) displaying greater amplitude than the 8 and 12-day cycles (attributable to short period pulses in lava effusion; Loughlin et al., 2010; Wadge et al., 2010).

Table 3
Significant cycles identified in OMI and MODIS observations of SHV and suggested causes.

Cycle period (days)	Instrument	Potential cause	Reference(s) to identified cycles
238	MODIS (night)	Volcanic—Dome collapse events and associated rock falls and LP earthquakes	Lamb et al. (2014)
172–182	MODIS	Meteorological—Bimodal wet season precipitation, troughs correspond to precipitation maxima	Barclay et al., 2006 Taylor et al. 2002
159	OMI	Volcanic—Meteorological influence ruled out therefore this cycle is most likely volcanic in origin	–
121	OMI	Volcanic—Pulsatory magma injection manifested by LP earthquakes	Lamb et al. (2014)
102	OMI	Volcanic—Cycle identified in the VT earthquake record at SHV	Lamb et al. (2014)
65–75	MODIS (night)	Volcanic—Extension of the 54–58 day cycle following major dome collapse events	–
54–58	MODIS OMI	Volcanic—Conduit dimensions causing pauses in emission due to renewed ascent following eruption	Costa et al. (2007) Lamb et al. (2014) Nicholson et al. (2013) Odbert et al. (2014) Sparks and Young, (2002) Vitturi et al. (2013)
11–12	OMI	Volcanic—Pulsatory lava effusion generating rockfalls and corresponding LP earthquakes related to dome growth and degassing	Loughlin et al. (2010) Nicholson et al. (2013) Wadge et al. (2010)
7–8	OMI	Satellite viewing angle—ORA patterns indicate ~8 day cycles in GIFOV geometry	–
2–4	MODIS (day) OMI	Satellite viewing angle—variations in GIFOV	–

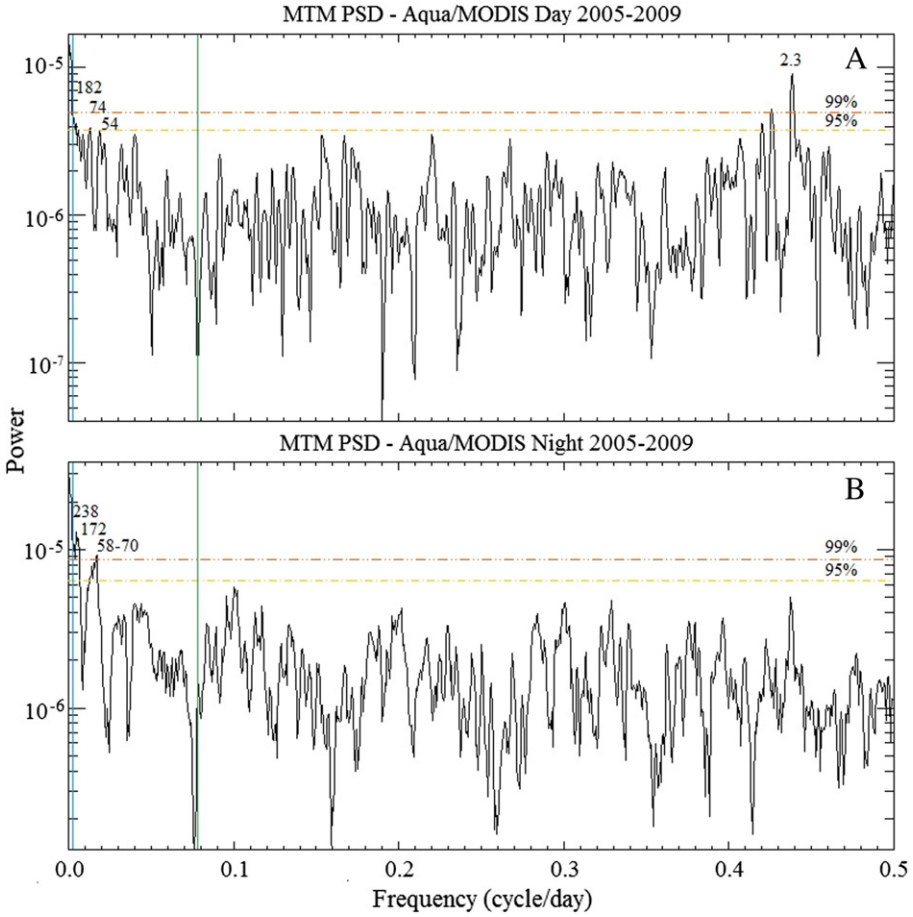

Fig. 3. MTM PSD plots of filtered MODIS data (daytime and night-time respectively) from Soufriere Hills during heightened activity (2005–2009) with corresponding 95% and 99% confidence levels indicating the relative significance of cycles identified. A LOD (-) of 450 days was used and is included (-) to indicate the maximum length of cycle considered. The satellite repeat cycle (16 days) is also indicated (-), as shorter-period (higher frequency) cycles could be artefacts of the measurement technique and hence require greater scrutiny.

The identification of the 55-day cycle using satellite data, in agreement with previously observed and modelled cycles based on ground-based measurements (Nicholson et al., 2013), indicates the versatility and effectiveness of this analysis as a tool for monitoring temporal changes in the dynamics of SHV, and potentially other volcanoes with adequate observational datasets. In order to validate the ability of our methodology to account for any temporal offset in the identified signals, a reconstruction of the ~55 day cycle was compared with an initiation point of the multi-week cycle previously established as occurring on or around February 10, 2006 by Odbert et al. (2014). In order to test the validity of our selection procedures, the ~55–58 day cycle was selected from the OMI and night-time MODIS analyses using the aforementioned bandpass filter technique (Section 3.2), with Fig. 5 displaying the relative forcing of these signals over time, in order to assess whether the reconstruction displayed similar characteristics to cycles identified in previous analyses. Fig. 5 indicates that the initiation of the multi-week cycle in the MODIS TIR dataset occurs within the timeframe identified by Odbert et al. (2014); but the SO_2 cyclicity

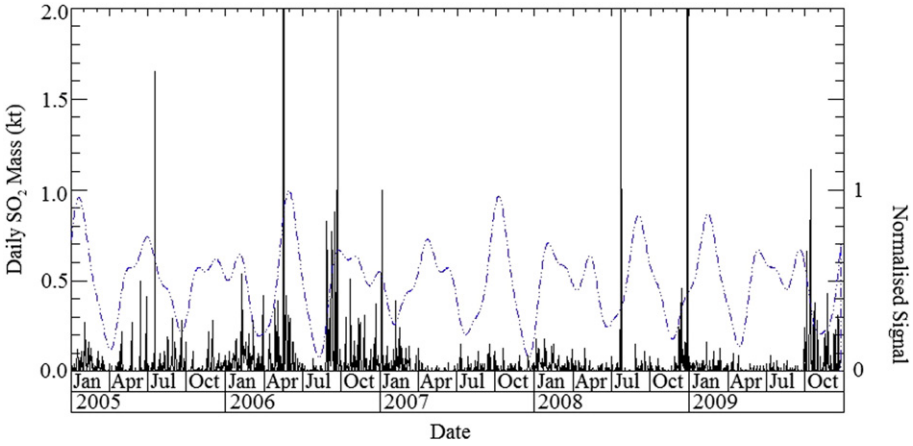

Fig. 4. Time series plot of OMI SO_2 observations for January 2005–December 2009, overlaid with a signal reconstruction (–) comprised of the 4 most significant cycles (with periods of 159, 121, 102, and 55 days).

displays an inverse pattern to the TIR reconstruction during this period. This could be a result of the limited ability of the methodology to account for variable cycle duration over time; which is common in natural systems. Despite the anti-phase nature of the OMI and MODIS cycles, individual eruptive events identified in the seismic record by Odbert et al. (2014) coincide with peaks in the 55-day cycle in the SO_2 record (25th December 2005, 7th February 2006, 5th April 2006, 20th May 2006, 8th September 2006, 5th November 2006, 25th December 2006 and 28th February 2007) and the 58-day cycle in the TIR data (24th October 2005, 25th December 2005, 25th June 2006, 18th August 2006, and 28th February 2007). A possible reason for the offset in the reconstructed SO_2 and TIR cycles is the impact of the 20th May 2006 dome collapse,, which corresponds to a peak in predicted SO_2 mass (Fig. 5), resulting from the large associated SO_2 discharge and subsequent depressurisation of the system. The TIR reconstruction, however, designates an initiation point for a new cycle at this time (Fig. 5), indicating a predicted upsurge in TIR emission due to extrusion of fresh lava dome material. However, coincident TIR data display minimal activity (Fig. 1, 6), most likely due to nascent dome growth in the May 2006 dome collapse scar being obscured in MODIS observations (Section 5). The resolution of these events through analysis of the reconstruction validates the potential extension of this technique to other volcanic systems with multi-annual records of SO_2 emissions detected from space.

4.32. Daytime MODIS

The analysis of daytime Aqua/MODIS data for SHV (2005–2009) identified two peaks in cyclical activity surpassing the 99% confidence limit (with periods of 2.28 and 2.34 days; Table 2). As previously stated, we disregarded cycles with periods exceeding the LOD (450 days), which eliminated a possible 500-day cycle. The remaining two cycles were selected using a bandpass filter and investigated for significance in the reconstruction analysis. Although these cycles have very similar periods, they appear as distinct peaks in the PSD spectra (Fig. 3) and were analysed in an attempt to identify which cycle displayed the dominant characteristics (2.34 days) and which represented the offset (2.28 days) resulting from variations in the timing of cyclic activity common in natural systems. We attribute these ~2.3-day cycles to periodic variations in the MODIS viewing angle during a 16-day satellite repeat cycle. This feature is also identifiable in the post-ORA OMI data analysis in Fig. 2, where the 2.3 day cycle is the most significant resolvable cycle, and therefore can be regarded as a systematic feature of the satellite measurements. Due to the high frequencies of these short-period cycles the resulting reconstruction resembles noise, therefore all cycles exceeding the 95% confidence level (periods of 182, 74, 54 and 2.38 days; Table 2) were also selected for comparison.

Following the incorporation of these less significant cycles the reconstructed signal correlates with periods of heightened activity at SHV (e.g., February–May 2006, September–October 2006: Fig. 6). Correlations between the reconstructed signal and the observations are likely the result of inclusion of the 54-day cycle, which correlates with the multi-week cycles identified and discussed in Section 4.31. Following investigation of the 74-day cycle, we propose that this is a result of shifts in the length of the multi-week cycle resulting from pauses in eruptive activity at SHV as well as major eruptive events that cause the system to destabilise. The 182-day cycle also contributes significantly to the correlation of observed activity and developed reconstruction due to annual peaks in February and August, but we attribute this cycle to regional meteorology, where wet season precipitation maxima correspond to minima in the projected cycles of TIR emission. The location of Montserrat at the edge of the Inter-tropical Convergence Zone (ITCZ) results in a consistent rainy season (April–November), but the Caribbean commonly displays bimodal characteristics, with peaks in rainfall in May–June and October (Taylor et al., 2002) resulting from a combination of precipitation driven by both cyclonic systems (hurricanes) and convective storms (Barclay et al., 2006). This results in an initial peak in precipitation in May and a secondary larger peak in October/November, during which time satellite observations of volcanic activity would be obscured by persistent cloud coverage. The intervals between the May and October peaks represent two periods of ~180 days and we therefore consider these to be the source of the identified 182-day cycle.

Despite the inclusion of cycles related to known driving forces at SHV, the reconstruction still fails to resolve many of the features displayed by the observations; for example the increased signals in April, September and November 2006 correspond to reduced signal in the reconstruction (Fig. 6). Conversely in June–August 2006 and December 2006–January 2007 the reconstruction predicts an increase in signal that is not observed, but these periods follow or include

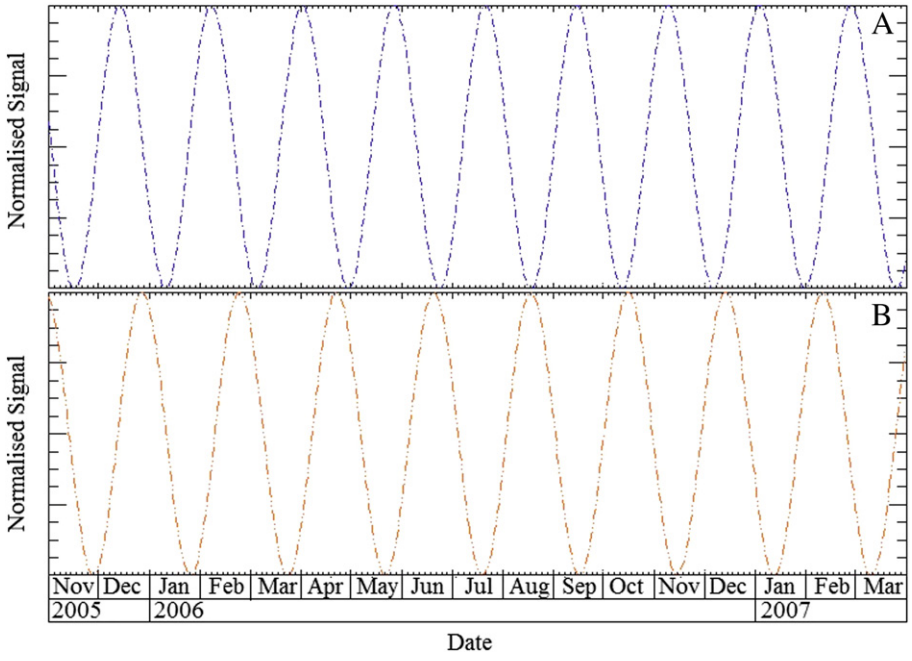

Fig. 5. Time series plot for November 2005–March 2007 of: A. Reconstructed 55 day cycle identified in the OMI SO_2 data; B. Reconstructed 58 day cycle identified in the MODIS data at SHV.

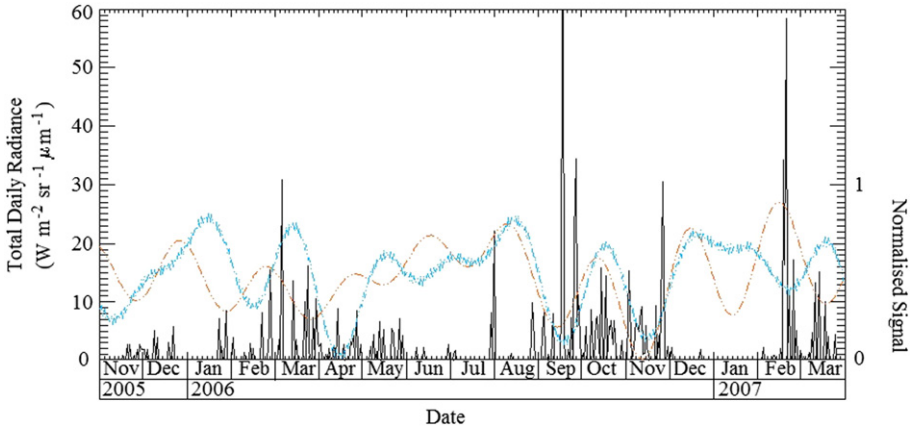

Fig. 6. MODIS observations of TIR radiance with reconstructions comprising cycles identified in daytime (blue) and night-time (red) MODIS datasets.

known dome collapse (20th May 2006; Wadge et al., 2014) and explosive destabilisation events (8th January 2007; De Angelis et al.2007), when reduced levels of TIR radiance (due to the absence of a large, active lava dome) would be expected (Section 4.33). However, the limitations of daytime MODIS data, which may have prevented the identification of more subtle variations in radiant intensity at SHV prompted a separate investigation of night-time data.

4.33. Night-time MODIS

Analysis of the night-time MODIS data revealed three PSD peaks below the LOD and surpassing the 99% confidence limit (238, 172, and 58 days) and 2 cycles greater than the 95% confidence limit (70 and 65 days; Table 2). By combining of the three dominant cycles (238, 172, and 58 days), some success was achieved in reconstructing the general TIR radiance signal (Fig. 6). The 58-day cycle corresponds to the multi-week cycle previously identified as a 54–55 day cycle in OMI and daytime MODIS data. We also ascribe the 65- and 70-day cycles to interruption of this cycle following large dome collapse events. The 172-day cycle displays similar characteristics to the 182-day cycle discussed in Section 4.32, and hence we attribute this to the waxing and waning of the wet season (Table 2, 3). A 238-day cycle identified in the night-time MODIS analysis is not apparent in either the OMI or daytime MODIS data; however, Lamb et al. (2014) identified a similar cycle in the long period (LP) earthquake record at SHV. The restriction of this cycle to the night-time MODIS observations implies that it is likely the result of activity that generates relatively low levels of TIR radiance. Weak signals cannot be detected in daytime MODIS overpasses, when the MODVOLC detection threshold is higher due to interference from solar reflection and heating (http://modis.higp.hawaii.edu/daytime.html). We therefore posit that this cycle is generated by rockfalls and small dome destabilisation events resulting in only minor exposure of the hot lava dome, or deposition of rockfall talus which cools rapidly precluding detection by the daytime MODVOLC algorithm but sufficient to trigger a night-time thermal alert. Loughlin et al (2010) also identified connections between LP earthquakes and rockfall events on shorter timescales (12 days), providing support for a link between observed cycles in LP earthquake data (Lamb et al., 2014) and night-time MODIS data on longer timescales.

As with the MODIS daytime reconstruction, following explosive events (June–August 2006 and December 2006–January 2007) the night-time MODIS data is characterised by minimal thermal anomaly detection, whereas the night-time reconstruction predicts an increase in signal (Fig. 6). This disagreement explored further in the discussion (Section 5). When compared to the daytime reconstruction (Fig. 6), we note that the night-time analysis provides better correlation with observations in April 2006 and February–March 2007 an increase in observed TIR radiance corresponds to an increase in the night-time reconstruction which is not captured in the daytime analysis. Mismatches between the reconstructed signal and the observations, such as in September and November 2006 where the reconstruction displays minimal forcing whilst the MODIS observation indicate an increase in radiant intensity, could be the result of the exclusion of longer period, lower frequency cycles from the reconstruction due to the imposed LOD.

4.34. Combined day/night time reconstruction

Following analysis of the separate daytime and night-time MODIS datasets, a combined reconstruction was generated using a combination of the cycles identified in the individual analyses in an attempt to better reconstruct the dynamics of TIR anomaly detection at SHV. This reconstruction involved a combination of the 54-day cycle from the daytime MODIS analysis and the 238-, 172- and 65 day cycles from the night-time MODIS analysis (Fig. 7b). Although this reconstruction still deviates from the observed TIR signal in June–August 2006 and December 2006–January 2007 (Section 5), corresponding peaks in activity and the reconstruction occur in November–December 2005, January–February 2006, March 2006, August 2006, October 2006 and February–March 2007 (Fig. 7b).

5. Discussion

To assess whether particular activity or eruptive dynamics can be distinguished from comparison of cyclical output, a shorter time period was selected to maximize data availability (November 2005–March 2007; Fig. 7) during a period encompassing multiple explosive or dome collapse events (Wadge et al., 2014). This permits assessment of the influence of system destabilisation on the correlation between observations and the developed reconstructions. A key discontinuity was identified between the reconstructions and the SO_2 and TIR observations in May–October 2006 (Fig. 7), which is most probably linked to the major dome collapse on 20th May 2006 (Global Volcanism Program, 2006; Wadge et al., 2014). Based on our reconstructions, an increase in the SO_2 emissions and TIR radiance was predicted in May–July 2006, but following the 20th May 2006 dome collapse a decrease in signal strength was observed. A likely reason for this discrepancy is the removal of the large pre-existing lava dome, and the venting of large amounts of SO_2 during the collapse (Carn and Prata, 2010). Following a period of anomalies related to the dome collapse and its deposits, the removal of the lava dome reduces the number of persistent TIR anomalies detected and SO_2 emissions decline. Lava dome growth did in fact continue at high extrusion rates immediately after the collapse (Wadge et al., 2010; Global Volcanism Program, 2006), and the predicted

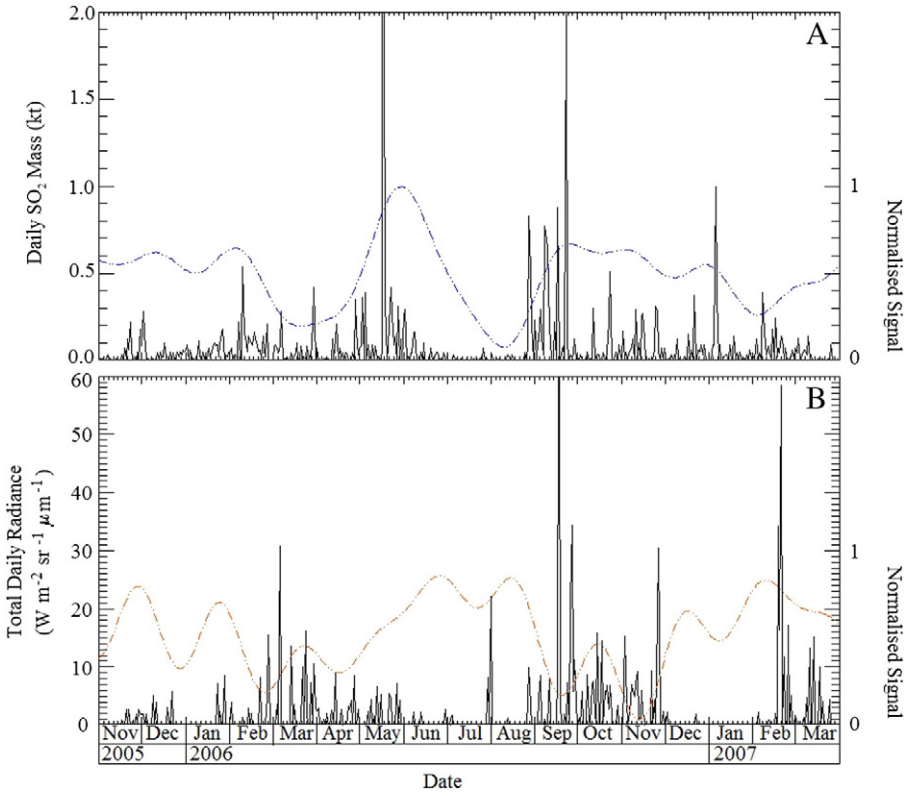

Fig. 7. Time series plot for November 2005–March 2007 of a) OMI SO_2 observations overlaid with a signal reconstruction (blue) comprised of the four selected cycles (159, 121, 102 and 55 days). b) MODIS radiance observations overlaid with a signal reconstruction (red) comprised of the four selected cycles (238, 172, 79 and 58 days) from a combination of both day and night-time MODIS data.

increase in TIR radiance may reflect this (Fig. 7), assuming that cycles in TIR emission correlate with episodes of dome growth. However, since the new lava dome grew within the May 20, 2006 collapse scar, satellite viewing angle constraints (coupled with the small size of the nascent dome) likely prevented detection of significant TIR radiance by MODIS in this period, until the dome once again surmounted the SHV crater rim and became 'visible' to the satellite at multiple viewing angles. Based on dome elevation data in Wadge et al. (2010), this occurred sometime in September–October 2006, which is consistent with a resurgence in TIR radiance in that period (Fig. 7). Regarding the SO_2 emissions, the 20th May 2006 collapse generated the largest instantaneous SO_2 emission of the entire SHV eruption to date (~0.2 Tg; Carn and Prata, 2010) and hence may have effectively 'flushed' the conduit system of SO_2. This may have prevented any subsequent increase in SO_2 emissions, which was predicted from the cyclic behaviour identified in the OMI record (Fig. 7), due to a shortage of SO_2 supply from depth. A reduction in SO_2 emissions post-collapse is also supported by ground-based SO_2 data; although no SO_2 data are available from late May until early July, SO_2 emission rates were subsequently rather low (Christopher et al., 2010), suggesting that the system required time to recharge with SO_2 supplied from depth (Edmonds et al., 2003).

6. Conclusion

Spectral analysis of OMI SO_2 measurements at SHV using the MTM technique reveals cyclic variations on similar timescales to those found in previous studies of surface deformation (Costa et al., 2007; Odbert and Wadge, 2009; Voight et al., 1998) and seismic data (Lamb et al., 2014; Odbert et al, 2014), with the most pronounced similarities (periods of 54, 12, and 8 days) to cycles identified in ground-based DOAS SO_2 data by Nicholson et al. (2013). The agreement between cyclical patterns of activity identified in our analysis and the work of Nicholson et al. (2013) implies that, whilst the absolute amounts of SO_2 detected differ considerably between ground-based and satellite measurements, similar eruptive dynamics are being observed by each technique. Our analysis provides further confirmation of the existence of a multi-week (~50 day) cycle at SHV, and also validates the use of satellite SO_2 measurements to investigate cyclical processes at other, less well-monitored volcanoes with suitable time-series of SO_2 data. Three additional cycles were also identified in the OMI SO_2 time-series at periods of 102-, 121- and 159 days which have been attributed to volcanic processes.

Inter-comparison of OMI SO_2 and MODIS TIR data at SHV reveals similarities in identified cycles, with all datasets showing cyclicity on timescales of ~55 days. Analysis of the combined day- and night-time MODIS data indicates that the night-time signals dominate, most likely due to the different MODVOLC algorithm thresholds used for day- and night-time observations. However, separate treatment of day- and night-time MODIS data facilitates the coincident assessment with OMI data and highlights distinct features of the SO_2 and TIR measurements. Analysis of night–time MODIS data reveals a 238-day cycle similar to that identified in the LP seismic record at SHV by Lamb et al. (2014). The synergistic use of SO_2 and TIR measurements permits resolution of more cycles and therefore provides more insight into volcanic processes than a single dataset.

Through the comparison of normalised OMI and MODIS signals we were able to identify periods displaying dynamic shifts in the observed activity at SHV, such as the dome collapse event of May 2006. This method could potentially be adapted to anticipate expected periods of increased activity in systems with relatively stable dynamics through the future projection of cycles identified in this manner; however, sufficient historical data would be required to facilitate initial cycle identification and assess their significance. During phase 5 of the eruption of SHV, the Montserrat Volcano Observatory employed this method of forecasting, based upon observed cyclicity, where personnel and equipment were deployed into the field prior to an expected increase

in activity with moderate success (Odbert et al, 2014). The significant reduction in activity following the time period studied herein indicates a distinct shift in the dynamics of the SHV system at and therefore future projection of the identified cycles is unlikely to be appropriate in this case. The near-global daily coverage provided by OMI and MODIS with measurements spanning over 10 years makes these platforms suitable for the assessment of cyclic behaviour at active volcanic systems worldwide. In addition to a data record of sufficient duration, a certain degree of stability is required within the volcanic system to ensure that cycles identified in prior observations are relevant to the future dynamics of the system.

Acknowledgments

We acknowledge NASA for supporting this work through the Aura Science Team project (grant NNX11AF42G) and an Earth and Space Science Fellowship to VJBF (NNX14AK94H). We would also like to thank H. Odbert for his thorough review that greatly improved this paper.

References

Barclay, J., Johnstone, J.E., Matthews, A.J., 2006. Meteorological monitoring of an active volcano: implications for eruption prediction. J. Volcanol. Geotherm. Res. 150 (4), 339–358.

Carn, S.A., Prata, F.J., 2010. Satellite-based constraints on explosive SO_2 release from Soufrière Hills Volcano, Montserrat. Geophys. Res. Lett. 37 (19). http://dx.doi.org/10.1029/2010GL044971.

Carn, S.A., Watts, R.B., Thompson, G., Norton, G.E., 2004. Anatomy of a lava dome collapse: the 20 March 2000 event at Soufrière Hills Volcano, Montserrat. J. Volcanol. Geotherm. Res. 131 (3), 241–264. http://dx.doi.org/10.1016/S0377-0273(03)00364-0.

Carn, S.A., Krueger, A.J., Krotkov, N.A., Yang, K., Levelt, P.F., 2007. Sulfur dioxide emissions from Peruvian copper smelters detected by the Ozone Monitoring Instrument. Geophys. Res. Lett. 34 (9). http://dx.doi.org/10.1029/2006GL029020.

Carn, S.A., Krotkov, N.A., Yang, K., Krueger, A.J., 2013. Measuring global volcanic degassing with the Ozone Monitoring Instrument (OMI). Geol. Soc. Lond., Spec. Publ. 380 (1), 229–257. http://dx.doi.org/10.1144/SP380.12.

Christopher, T., Edmonds, M., Humphreys, M.C.S., Herd, R.A., 2010. Volcanic gas emissions from Soufrière Hills Volcano, Montserrat 1995 – 2009, with implications for mafic magma supply and degassing. Geophys. Res. Lett. 37. http://dx.doi.org/10.1029/2009GL041325 (L00E04).

Costa, A., Melnik, O., Sparks, R.S.J., Voight, B., 2007. Control of magma flow in dykes on cyclic lava dome extrusion. Geophys. Res. Lett. 34 (2). http://dx.doi.org/10.1029/2006GL027466.

Costa, A., Wadge, G., Stewart, R., Odbert, H., 2013. Coupled subdaily and multiweek cycles during the lava dome eruption of Soufrière Hills Volcano, Montserrat. J. Geophys. Res. Solid Earth 118 (5), 1895–1903. http://dx.doi.org/10.1002/jgrb.50095.

De Angelis, S., Bass, V.A., Hards, V.L., Ryan, G.A., 2007. Seismic characterisation of pyroclastic flow activity at Soufrière Hills Volcano, Montserrat, 8 January 2007. Nat. Hazards Earth Syst. Sci. 7 (4), 467–472.

Denlinger, R.P., Hoblitt, R.P., 1999. Cyclic eruptive behavior of silicic volcanoes. Geology 27 (5), 459–462. http://dx.doi.org/10.1130/0091-7613(1999)027<0459:CEBOSV>2.3.CO;2.

Druitt, T.H., Young, S.R., Baptie, B., Bonadonna, C., Calder, E.S., Clarke, A.B., Cole, P.D., Harford, C.L., Herd, R.A., Luckett, R., Ryan, G., Voight, B., 2002. Episodes of cyclic Vulcanian explosive activity with fountain collapse at Soufrière Hills Volcano, Montserrat. Geol. Soc. Lond. Mem. 21, 281–306.

Duchon, C., Hale, R., 2012. Time Series Analysis in Meteorology and Climatology: An Introduction. Advancing Weather and Climate Science. Wiley.

Edmonds, M., Oppenheimer, C., Pyle, D.M., Herd, R.A., Thompson, G., 2003. SO_2 emissions from Soufrière Hills Volcano and their relationship to conduit permeability, hydrothermal interaction and degassing regime. J. Volcanol. Geotherm. Res. 124 (1), 23–43. http://dx.doi.org/10.1016/S0377-0273(03)00041-6.

Elsworth, D., Mattioli, G., Taron, J., Voight, B., Herd, R., 2008. Implications of magma transfer between multiple reservoirs on eruption cycling. Science 322 (5899), 246–248.

Giglio, L., Descloitres, J., Justice, C.O., Kaufman, Y.J., 2003. An enhanced contextual fire detection algorithm for MODIS. Remote Sens. Environ. 87 (2), 273–282. http://dx.doi.org/10.1016/S0034-4257(03)00184-6.

Global Volcanism Program, 2006. Report on Soufrière Hills (United Kingdom). In: Wunderman, R. (Ed.), Bulletin of the Global Volcanism Network, 31:5. Smithsonian Institution http://dx.doi.org/10.5479/si.GVP.BGVN200605-360050.

Global Volcanism Program, 2009. Report on Soufrière Hills (United Kingdom). In: Wunderman, R. (Ed.), *Bulletin of the Global Volcanism Network*, 34:10. Smithsonian Institution http://dx.doi.org/10.5479/si.GVP.BGVN200910-360050.

Jaquet, O., Carniel, R., Sparks, S., Thompson, G., Namar, R., Di Cecca, M., 2006. DEVIN: a forecasting approach using stochastic methods applied to the Soufriere Hills Volcano. J. Volcanol. Geotherm. Res. 153 (1), 97–111.

Koeppen, W.C., Pilger, E., Wright, R., 2011. Time series analysis of infrared satellite data for detecting thermal anomalies: a hybrid approach. Bull. Volcanol. 73 (5), 577–593. http://dx.doi.org/10.1007/s00445-010-0427-y.

Komorowski, J.C., Legendre, Y., Christopher, T., Bernstein, M., Stewart, R., Joseph, E., Fournier, N., Chardot, L., Finizola, A., Wadge, G., Syers, R., Williams, C., Bass, V., 2010. Insights into processes and deposits of hazardous vulcanian explosions at Soufrière Hills Volcano during 2008 and 2009 (Montserrat, West Indies). Geophys. Res. Lett. 37 (19).

Krotkov, N.A., Carn, S.A., Krueger, A.J., Bhartia, P.K., Yang, K., 2006. Band residual difference algorithm for retrieval of SO_2 from the Aura Ozone Monitoring Instrument (OMI). IEEE Trans. Geosci. Remote Sens. 44 (5), 1259–1266.

Krotkov, N.A., Schoeberl, M.R., Morris, G.A., Carn, S., Yang, K., 2010. Dispersion and lifetime of the SO_2 cloud from the August 2008 Kasatochi eruption. J. Geophys. Res.-Atmos. 115 (D2). http://dx.doi.org/10.1029/2010JD013984.

Lamb, O.D., Varley, N.R., Mather, T.A., Pyle, D.M., Smith, P.J., Liu, E.J., 2014. Multiple time-scales of cyclical behaviour observed at two dome-forming eruptions. J. Volcanol. Geotherm. Res. 284, 106–121.

Lensky, N.G., Sparks, R.S.J., Navon, O., Lyakhovsky, V., 2008. Cyclic activity at Soufrière Hills Volcano, Montserrat: degassing-induced pressurization and stick–slip extrusion. Geol. Soc. Lond., Spec. Publ. 307 (1), 169–188.

Loughlin, S.C., Luckett, R., Ryan, G., Christopher, T., Hards, V., De Angelis, S., ... Strutt, M., 2010. An overview of lava dome evolution, dome collapse and cyclicity at Soufrière Hills Volcano, Montserrat, 2005–2007. Geophys. Res. Lett. 37 (19). http://dx.doi.org/10.1029/2010GL042547.

Mann, M.E., Lees, J.M., 1996. Robust estimation of background noise and signal detection in climatic time series. Clim. Chang. 33 (3), 409–445.

McCormick, B.T., Edmonds, M., Mather, T.A., Carn, S.A., 2012. First synoptic analysis of volcanic degassing in Papua New Guinea. Geochem. Geophys. Geosyst. 13 (3).

Melnik, O., Sparks, R.S.J., 2005. Controls on conduit magma flow dynamics during lava dome building eruptions. J. Geophys. Res. Solid Earth 110 (B2).

Michaut, C., Ricard, Y., Bercovici, D., Sparks, R.S.J., 2013. Eruption cyclicity at silicic volcanoes potentially caused by magmatic gas waves. Nature Geoscience 6 (10), 856–860. http://dx.doi.org/10.1038ngeo1928.

NASA, 2010. A-Train. www.nasa.gov/mission_pages/a-train/a-train.html.

Nicholson, E.J., Mather, T.A., Pyle, D.M., Odbert, H.M., Christopher, T., 2013. Cyclical patterns in volcanic degassing revealed by SO_2 flux timeseries analysis: an application to Soufrière Hills Volcano, Montserrat. Earth Planet. Sci. Lett. 375, 209–221.

Odbert, H.M., Wadge, G., 2009. Time series analysis of lava flux. J. Volcanol. Geotherm. Res. 188 (4), 305–314.

Odbert, H.M., Stewart, R.C., Wadge, G., 2014. Cyclic phenomena at the Soufrière Hills volcano, Montserrat. Geol. Soc. Lond. Mem. 39 (1), 41–60.

Percival, D.B., Walden, A.T., 1993. Spectral analysis for physical applications. Cambridge University Press.

Platt, U., Stutz, J., 2008. *Differential Absorption Spectroscopy* (pp. 135–174). Springer, Berlin Heidelberg.

Prata, A.J., Carn, S.A., Stohl, A., Kerkmann, J., 2007. Long range transport and fate of a stratospheric volcanic cloud from Soufriere Hills volcano, Montserrat. Atmos. Chem. Phys. 7 (19), 5093–5103.

Spampinato, L., Oppenheimer, C., Cannata, A., Montalto, P., Salerno, G.G., Calvari, S., 2012. On the time-scale of thermal cycles associated with open-vent degassing. Bull. Volcanol. 74 (6), 1281–1292.

Sparks, R.S.J., Young, S.R., 2002. The eruption of Soufrière Hills volcano, Montserrat (1995–1999): overview of scientific results. Geol. Soc. Lond. Mem. 21 (1), 45–69.

Taylor, M.A., Enfield, D.B., Chen, A.A., 2002. Influence of the tropical Atlantic versus the tropical Pacific on Caribbean rainfall. J. Geophys. Res. Oceans 107 (C9), 10–11.

Thomson, D.J., 1982. Spectrum estimation and harmonic analysis. Proc. IEEE 70 (9), 1055–1096.

Vitturi, M.D.M., Clarke, A.B., Neri, A., Voight, B., 2013. Extrusion cycles during dome-building eruptions. Earth Planet. Sci. Lett. 371, 37–48. http://dx.doi.org/10.1016/j.epsl.2013.03.037.

Voight, B., Hoblitt, R.P., Clarke, A.B., Lockhart, A.B., Miller, A., Lynch, L., McMahon, J., 1998. Remarkable cyclic ground deformation monitored in real-time on Montserrat, and its use in eruption forecasting. Geophys. Res. Lett. 25 (18), 3405–3408.

Voight, B., Sparks, R.S.J., Miller, A.D., Stewart, R.C., Hoblitt, R.P., Clarke, A., Ewart, J., Aspinall, W.P., Baptie, B., Calder, E.S., Cole, P., Druitt, T.H., Hartford, C., Herd, R.A., Jackson, P., Lejeune, A.M., Lockhart, A.B., Loughlin, S.C., Luckett, R., Lynch, L., Norton, G.E., Robertson, R., Watson, I.M., Watts, R., Young, S.R., 1999. Magma flow instability and cyclic activity at Soufriere hills volcano, Montserrat, British west indies. Science 283 (5405), 1138–1142.

Wadge, G., Herd, R., Ryan, G., Calder, E.S., Komorowski, J.C., 2010. Lava production at Soufrière Hills Volcano, Montserrat: 1995–2009. Geophys. Res. Lett. 37 (19).

Wadge, G., Voight, B., Sparks, R.S.J., Cole, P.D., Loughlin, S.C., Robertson, R.E.A., 2014. An overview of the eruption of Soufriere Hills Volcano, Montserrat from 2000 to 2010. Geol. Soc. Lond. Mem. 39 (1), 1–40.

Watson, I.M., Oppenheimer, C., Voight, B., Francis, P.W., Clarke, A., Stix, J., Miller, A., Pyle, D.M., Burton, M.R., Young, S.R., Norton, G., Loughlin, S., Darroux, B., Staff, M.V.O., 2000. The relationship between degassing and ground deformation at Soufriere Hills Volcano, Montserrat. J. Volcanol. Geotherm. Res. 98 (1), 117–126.

Wooster, M.J., Rothery, D.A., Kaneko, T., 1998. Geometric considerations for the remote monitoring of volcanoes: studies of lava domes using ATSR and the implications for MODIS. Int. J. Remote Sens. 19 (13), 2585–2591.

Wright, R., Flynn, L., Garbeil, H., Harris, A., Pilger, E., 2002. Automated volcanic eruption detection using MODIS. Remote Sens. Environ. 82 (1), 135–155.

Wright, R., Flynn, L.P., Garbeil, H., Harris, A.J., Pilger, E., 2004. MODVOLC: near-real-time thermal monitoring of global volcanism. J. Volcanol. Geotherm. Res. 135 (1), 29–49.

Yang, K., Krotkov, N.A., Krueger, A.J., Carn, S.A., Bhartia, P.K., Levelt, P.F., 2007. Retrieval of large volcanic SO_2 columns from the Aura Ozone Monitoring Instrument: comparison and limitations. J. Geophys. Res.-Atmos. 112 (D24).

Yang, K., Krotkov, N.A., Krueger, A.J., Carn, S.A., Bhartia, P.K., Levelt, P.F., 2009. Improving retrieval of volcanic sulfur dioxide from backscattered UV satellite observations. Geophys. Res. Lett. 36 (3).